Contrib Mineral Petrol (2016) 171:84
DOI 10.1007/s00410-016-1296-y

ORIGINAL PAPER

Experimental subsolidus phase relations in the system $CaCO_3$–$CaMg(CO_3)_2$ up to 6.5 GPa and implications for subducted marbles

Jörg Hermann[1,2] · **Ulrike Troitzsch**[1] · **Dean Scott**[1]

Received: 24 June 2016 / Accepted: 2 September 2016 / Published online: 24 September 2016

Abstract The dissociation of dolomite to aragonite + magnesite and the reaction of dolomite + aragonite to Mg-calcite have been experimentally determined by piston cylinder experiments in the range of 650–1000 °C and 2–6.5 GPa. Friction decay within the salt sleeves used as pressure medium was monitored by continuously logging the travel distance of the piston. Piston movement ceased after the first 24 h of the experiment, and all experiments were kept at the steady-state conditions for an additional 24–196 h. The reaction of dolomite to aragonite + magnesite has a positive slope and has been bracketed at 650 °C between 5.1 and 5.8 GPa and at 750 °C between 5.7 and 6.5 GPa. The reaction is sluggish with a 0.6-GPa interval where all three phases coexist. The reaction dolomite + aragonite to Mg-calcite has been determined in 0.5-GPa intervals from 660 °C at 2 GPa to 940 °C at 6.5 GPa. The composition of Mg-calcite at the reaction curve is buffered and changes systematically from X(Ca) of 0.90 at 2 GPa to 0.57 at 6.5 GPa. The solvus between dolomite and Mg-calcite shrinks slightly with increasing pressure, providing evidence for a small negative slope of the critical curve dolomite = Mg-calcite. The degree of disorder in dolomite has been determined in some of the retrieved samples by Rietveld refinement based on X-ray diffraction patterns. The order parameter S decreases gradually from 1 to 0.7 as a function of temperature as the critical curve is approached and then drops dramatically after crossing it. No ordering on quench has been observed. The experimental results permit the construction of a petrogenetic grid for the system dolomite, aragonite, Mg-calcite, and magnesite, which has an invariant point at ~7.5 GPa and 980 °C, representing the maximum pressure stability of dolomite. X(Ca) isopleths of Mg-calcite coexisting with dolomite serve mainly as a thermometer, whereas in the presence of aragonite they are a useful barometer. The experimental results have been applied to diamond-bearing marbles of the Kokchetav Massif, where Mg-calcite inclusions in garnet and zircon with X(Ca) of 0.76 most likely formed during prograde metamorphism close to the graphite–diamond transition.

Keywords Mg-calcite · Experimental petrology · Subduction · Marbles · UHP metamorphism

Introduction

Carbonates in subducted sediments play a key role in the long-term CO_2 cycle (Caldeira 1991; Kelemen and Manning 2015), and thus, phase and melting relations in carbonates at high pressures have attracted a lot of attention. The observation of marbles in ultrahigh-pressure metamorphic (UHP) terrains demonstrates that carbonates are stable up to mantle pressures and temperatures (Becker and Altherr 1992). For example, in the Dora Maira Massif, Western Alps, dolomite and calcite marbles reached peak metamorphic conditions of ~4 GPa, 730 °C (Castelli et al. 2007), indicating that carbonates were subducted to more than 100 km depth before exhumation back to the surface. Even higher pressures and temperatures of ~5 GPa,

Communicated by Hans Keppler.

✉ Jörg Hermann
joerg.hermann@geo.unibe.ch

[1] Research School of Earth Sciences, The Australian National University, 6201 Canberra, Australia

[2] Institute of Geological Sciences, University of Bern, Baltzerstrasse 3, 3012 Bern, Switzerland

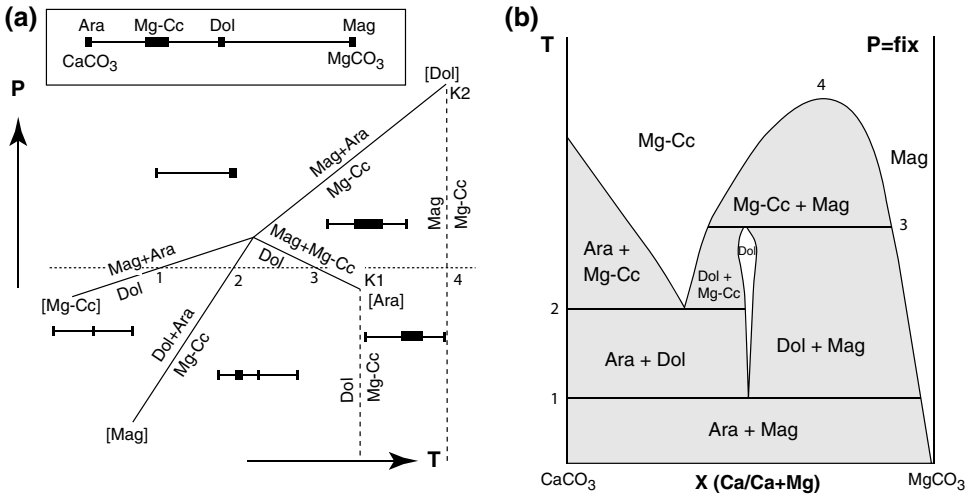

Fig. 1 **a** Schematic pressure (*P*)–temperature (*T*) phase relations in the $CaCO_3$–$MgCO_3$ system with the phases aragonite (Ara), Mg-calcite (Mg-Cc), dolomite (Dol), and magnesite (Mag). [Dol] denotes a reaction where dolomite is absent. K1 and K2 are critical points where a reaction line terminates because it intersects a critical curve (crest of the solvus). A schematic chemography is given for each divariant field. **b** Schematic temperature (*T*)–composition (*X*) diagram at a fixed pressure (*dashed line* in **a**). Numbers *1–3* refer to temperatures, where reaction lines are crossed. In divariant assemblages (two phases present, gray fields), the composition of phases is independent of the bulk composition

1000 °C are documented in marbles from the Kokchetav Massif, Kazakhstan, where additionally metamorphic diamond occurs (Sobolev and Shatsky 1990). One key question in carbonate-bearing UHP rocks is whether there is evidence for the dolomite dissociation into aragonite and magnesite (Dobrzhinetskaya et al. 2006; Proyer et al. 2013; Zhang et al. 2003). This univariant reaction would provide an excellent marker to constrain minimum pressures in deeply subducted marbles. There have been several experimental studies showing general agreement that this reaction occurs at UHP conditions (Buob et al. 2006; Hammouda et al. 2011; Luth 2001; Martinez et al. 1996; Morlidge et al. 2006; Sato and Katsura 2001). However, in detail the reaction curves differ by up to 2 GPa in the temperature range of 650–950 °C relevant for UHP rocks. It has been speculated that order–disorder in dolomite could be responsible for the large divergence of experimental results (Hammouda et al. 2011; Morlidge et al. 2006). Interestingly, a second reaction in the carbonate system, where ordered aragonite and dolomite react to the unordered Mg-calcite, has attracted much less attention. The formation of Mg-calcite from aragonite and dolomite has not been studied systematically since the work of Goldsmith and Newton (1969), who investigated this reaction up to 2.5 GPa. Mg-calcite has also been observed in diamond-bearing meta-carbonates of the Kokchetav massif (Ogasawara et al. 2000). These authors pointed out the importance of an experimental calibration of this reaction to pressures of 6 GPa in order to correctly interpret UHP dolomitic marbles.

In this paper, we determined the positions of both reactions up to 6.5 GPa using piston cylinder experiments. The run products were characterized compositionally with electron microprobe as well as structurally using Rietveld structure refinements from powder X-ray diffraction to assess to what extent order–disorder in dolomite influences the position of reactions. The implications of the experimental results for carbonate phase relations in UHP rocks will be discussed.

Phase petrology

The subsolidus Ca–Mg carbonate system at high pressure can be described by two components ($CaCO_3$ and $MgCO_3$) and the four phases aragonite (Ara), Mg-calcite (Mg-Cc), dolomite (Dol), and magnesite (Mag). The phase rule dictates that there is one invariant point in this system, and three phases must be present at each univariant line. This results in four univariant reactions that can be arranged using Schreinemakers rule (Fig. 1a). While aragonite, dolomite, and magnesite have a limited compositional range over most of the *P–T* diagram, Mg-calcite can vary enormously. The composition of all phases along a univariant line is fixed; thus, Mg-calcite continuously changes its composition along the reactions [Mag], [Dol], and [Ara]. The system is further complicated by the presence of three solvi (Irving and Wyllie 1975). The first solvus occurs between dolomite and Mg-calcite, the second between dolomite and magnesite, and the third between

Mg-calcite and magnesite. A schematic arrangement of the reaction lines and solvi is shown in a schematic *T*–*X* section (Fig. 1b), crossing three univariant lines. In any two-phase field, the composition of the phases is independent of the bulk and a function of the *P*–*T* conditions, whereas in one-phase fields the composition is a function of the bulk composition. Depending on the coexisting phase, the *X*(Ca) (Ca/Ca + Mg on molar basis) of Mg-Cc becomes higher (coexisting with aragonite) or lower (coexisting with dolomite) with increasing temperature. At the chosen pressure for the *T*–*X* diagram, the closure of the solvus is not encountered but instead is truncated by the reaction Dol = Mg-Cc + Mag. This reaction also truncates the Dol-Mag solvus. The reaction products form a solvus again that closes at very high temperatures. The projection of the crest of the solvus on the *P*–*T* plane defines a critical curve. The intersection of a critical curve with a reaction that contains both phases of a solvus produces a critical point, where the reaction terminates (e.g., Irving and Wyllie 1975). From these considerations, it is evident that in order to understand the subsolidus Ca–Mg carbonate system, it is important to study more than just one reaction. Moreover, the phase relations assist in the choice of starting materials for a given target region in *P*–*T* space. In this study, we focus on the join dolomite–aragonite with special emphasis on the reactions Dol = Mag + Ara and Dol + Ara = Mg-Cc.

Techniques

Starting materials

Starting materials were mixed from natural dolomite (Lengenbach, Switzerland; 0.17 wt% FeO), magnesite (Queensland, Australia; 0.8 wt% CaO, 0.02 wt% FeO), laboratory-grade $CaCO_3$ (AnalaR, better than 99.5 % pure), and aragonite, synthesized from $CaCO_3$ at 3 GPa, 600 °C. The starting material for experiments to constrain the reaction Dol = Ara + Mag consists of a mix with 50 mol % Dol, 25 % Ara, and 25 % Mag (Mix 1). This permits to run "reversal" experiments where it is possible to monitor the disappearance of the reactants and the formation of the products of the reaction at the same time. For the reaction Ara + Dol = Mg-Cc, dolomite and $CaCO_3$ were mixed in different proportions to produce 4 compositions (Mix 2–5) as indicated in Table 1. Aragonite formed easily in these experiments as shown by X-ray diffraction of the run products (Table 2), and thus, experiments were not run with pre-synthesized aragonite. Experiments close to the reaction line were run with a double composition consisting of 20 % Cc, 80 % Dol in one half of the capsule, and 80 % Cc and 20 % Dol in the other half, in an attempt to get "compositional reversals" for the composition of Mg-Cc at the reaction. Mix 6 consists of 50 % Cc and 50 % Mag and was used to synthesize a high-temperature, fully disordered carbonate with dolomite stoichiometry. 10 wt% of oxalic acid dihydrate ($H_2C_2O_4{\cdot}2H_2O$) has been added to all the mixes in order to flux the reactions. Oxalic acid dihydrate decomposes above 160 °C into 2 H_2O + 2 CO_2 + H_2.

Experiments

The starting material was loaded in platinum capsules of 2.3 mm outer diameter and placed into MgO inserts that were put within the graphite heater. Three different outer assemblies have been used (Table 1). For the high-pressure experiments at 650 °C, the graphite heater was inserted into an AgCl sleeve, which has the fastest friction decay (Assembly A, Table 1). At higher temperatures, AgCl starts melting and thus was replaced either by a NaCl-Pyrex (Assembly B) or by NaCl only sleeve. All assemblies were surrounded by Teflon foil to further minimize friction. The experiments were run in 1.27-cm-diameter vessels in piston cylinder apparatuses either using a 200T end-loaded press for experiments up to 3.5 GPa, or a 500T end-loaded press (called ultrahigh-pressure (UHP) piston cylinder) for the experiments up to 6.7 GPa. For the runs on the UHP piston cylinder, a prestressed Strecon vessel has been used. We have used 28.06-mm-long pistons of K8-grade tungsten carbide for UHP runs. After each run, the diameter of the piston was measured, and at the slightest sign of bulging, the piston was discarded. We have also investigated whether polishing the piston might help to prevent breakage, but no conclusive evidence was found on this issue. The piston travel in all ultrahigh-pressure piston cylinder experiments was monitored for the duration of the experiment with a Mitutoyo micrometer (accurate to 0.01 mm) that measures the movement between the bridge and the bottom plate of the press. Initially (H-runs of Table 1), the piston travel was checked periodically, and ram pressure was adjusted manually. In a further development, the piston cylinder was fully automated with logging of temperature, piston travel, and ram pressure every 2 s. Through a LabVIEW program, the ram pressure was adjusted automatically when needed. Figure 2a shows the nominal experimental pressure and piston travel through an experiment lasting for 4 days. For the first few hours, the piston traveled significantly, and frequent pump strokes were required to maintain the pressure constant, indicating friction decay of the assembly. Generally after 24 h, the piston travel reached a plateau, indicating that friction has dissipated and that the experiment reached steady state. Thus, pressure can be calculated from load and is accurate to ~0.1 GPa. All experiments were left for at least 24 h (most for 72 h or more) at this steady-state condition. Temperature was controlled using type B thermocouples ($Pt_{94}Rh_6/Pt_{70}Rh_{30}$) and is accurate to ±10 °C.

Table 1 Experimental conditions, starting materials, run products, and carbonate compositions for the two investigated reactions

Run		*P* (GPa)	*T* (°C)	Sm[a]	As[b]	Hours	Phases[c]	Ara	Mag *X* (Ca) × 100	Dol	MgCc
Dol -> Ara + Mag											
125	XRD	3	650	1	A	72	**Dol**, *Ara*, *Mag*				
126	XRD	3.5	650	1	A	144	**Dol**, *Ara*, *Mag*				
127	XRD	4	650	1	A	168	**Dol**, *Ara*, *Mag*				
128	XRD	4.6	650	1	A	144	**Dol**, *Ara*, *Mag*				
129	XRD	5.1	650	1	A	240	**Dol**, *Ara*, *Mag*		1.8		
130	XRD	5.4	650	1	A	264	**Dol**, *Ara*, *Mag*				
131	XRD	5.6	650	1	A	264	Dol, Ara, Mag				
132		5.8	650	1	A	216	**Ara**, **Mag**, *Dol*	100	1.9 (0.7)[d]		
143	XRD	5.65	750	1	A	96	**Dol**, *Ara*, *Mag*				
140	XRD	5.8	750	1	A	52	Dol, Ara, Mag				
H 158		6	750	1	B	168	Dol, Ara, Mag				
H167		6.3	750	1	B	168	Dol, Ara, Mag				
UHP158		6.5	750	1	C	48	**Ara**, **Mag**	100	2.6 (0.5)		
H152	XRD	6	850	1	B	144	**Dol**, *Ara*, *Mag*	100		50.6 (0.4)	
H161		6.5	850	1	B	168	**Dol**, *Ara*, *Mag*			49.7 (0.3)	
H165		6.7	850	1	B	120	**Dol**, *Ara*, *Mag*			49.7 (0.2)	
Dol + Ara -> Mg-Cc											
C-1916		2	650	2	B	168	**Dol**, **Ara**			51.3 (0.2)	
UHP 45		2	670	4	C	96	**MgCc**, **Dol**			50 (0.3)	88.8 (0.9)
UHP104		2.5	680	4	C	96	**MgCc**, **Dol**			49.8 (0.4)	90.8 (0.3)
UHP 46[f]		2.5	700	4	C	96	**MgCc**, *Ara*	n.a.[e]			88.9 (1.0)
UHP 46		2.5	700	4	C	96	**MgCc**, **Dol**			n.a.	86.9 (2.0)
C-2599		2.5	710	4	C	96	**Dol**, **MgCc**			49.6 (0.2)	84.7 (0.5)
C-2599		2.5	710	4	C	96	**MgCc**, *Ara*	n.a.			89 (0.7)
C-1915		3	700	2	B	168	**Dol**, **Ara**	100		50.7 (0.2)	
H146		3	725	2	B	168	**Dol**, **Ara**, *MgCc*	99.3		50.1 (0.4)	
UHP 47		3	740	4	C	96	**MgCc**, **Dol**			50.2 (1.7)	86.8 (2.4)
C-2589		3	750	2	C	168	**Dol**, **MgCc**			49.7 (0.3)	85.5 (1.6)
C-1911		3	800	2	B	196	**Dol**, **MgCc**			50 (0.3)	85.6 (1.6)
C-3268	XRD	3	1100	6	B	72	**MgCc**, Mag, *melt*		7 (1)		48.1 (0.8)
C-2584		3.5	760	2	C	50	**Ara**, **Dol**	99.8			
UHP 48		3.5	795	4	C	96	**MgCc**, **Dol**			49.5 (0.3)	80.3 (1.9)
D-736		3.5	810	2	C	168	**Dol**, **MgCc**			49.9 (0.3)	78.6 (0.8)
136	XRD	4	800	2	B	168	**Dol**, **Ara**, *MgCc*	100		50 (0.3)	
UHP 49		4	810	4	C	96	**Dol**, **Ara**				
138	XRD	4	825	2	B	96	**Dol**, **MgCc**, *Ara*			49.9 (0.2)	80.1 (0.7)
137	XRD	4	850	2	B	220	**Dol**, **MgCc**			49.8 (0.2)	75.6 (0.8)
135	XRD	4	900	2	B	72	**MgCc**				73.6 (0.7)
H147	XRD	4	1000	3	B	168	**MgCc**				62.8 (0.5)
UHP 133	XRD	4	1050	5	C	96	**MgCc**				59.3 (1.0)
UHP 50		4.5	850	4	C	96	**Ara**, **Dol**	99.8		49.6 (0.2)	
UHP 73		4.5	875	4	C	96	**Ara**, **MgCc**	99.7			72.7 (1.3)
H149		5	860	3	B	168	**Dol**, **Ara**	99.8		49.9 (0.3)	
H148		5	890	3	B	168	**Dol**, **MgCc**			49.8 (0.5)	71.5 (0.9)
UHP 40		5	890	4	C	96	**Ara**, **MgCc**	100			77.3 (0.6)
UHP 40		5	890	4	C	96	**MgCc**, **Dol**	100		49.8 (0.2)	70.3 (0.7)

Table 1 continued

Run		*P* (GPa)	*T* (°C)	Sm[a]	As[b]	Hours	Phases[c]	Ara	Mag *X* (Ca) × 100	Dol	MgCc
H150	XRD	5	950	3	B	168	**Dol**, **MgCc**			51 (0.2)	66.8 (0.8)
UHP 74		5	1000	4	C	96	**MgCc**, *Ara*				60–80
UHP 74		5	1000	4	C	96	**MgCc**				60–80
UHP 76		5.5	900	4	C	96	**Ara**, **Dol**	99.9		49.8 (0.2)	
UHP 77		5.5	925	4	C	96	**Ara**, **Dol**	99.9		49.9 (0.5)	
UHP 135		5.5	940	5	C	96	**Mg-Cc**, *melt*				58.9 (0.8)
UHP152		6	925	3	C	72	**MgCc**, *Ara*	100			60.4 (1.5)
H154	XRD	6	950	3	B	144	**Dol**, **MgCc**			50 (0.3)	64.4 (0.9)
UHP159		6.5	925	3	C	72	**Dol**, **Ara**				
UHP 154		6.5	950	3	C	72	**MgCc**				
UHP 136	XRD	6.5	975	5	C	96	**Mg-Cc**, *Dol*			52.6 (0.6)	57 (1.0)

[a] SM = starting material

Mix 1: 25 % aragonite, 50 % dolomite, 25 % magnesite

Mix 2: 50 % aragonite, 50 % dolomite

Mix 3: 25 % calcite, 75 % dolomite

Mix 4: 20 % calcite 80 % dolomite and 80 % calcite 20 % dolomite

Mix 5: 10 % Calcite, 90 % dolomite

Mix 6: 50 % Calcite, 50 % magnesite

[b] As = assembly

A: AgCl–graphite–MgO–Pt-capsule

B: NaCl–Pyrex–graphite–MgO–Pt-capsule

C: NaCl–graphite–MgO–Pt-capsule

[c] Main phases are shown in bold, minor phases in italics

[d] Standard deviation of multiple analyses in brackets

[e] n.a. = not analyzed

[f] For experiments with SM 4, the compositions are shown in consecutive rows only when the phase assemblages in the layers are different

At the termination of the experiment, power was switched off, which resulted in fast quenching of the experiment within less than 10 s (Fig. 2b). Generally, the piston traveled inward due to thermal contraction of the assembly on quenching (Fig. 2b). This provides evidence that the piston did not jam in the vessel during the UHP experiment.

Phase compositions

The phase relations were investigated with backscattered electron images (BSE) using a JEOL 6400 SEM (Centre of Advanced Microscopy, ANU) with EDS operating at 15 kV and a focussed beam of 1 nA. At such low beam current, the carbonates are stable. Carbonate compositions have been measured by wavelength-dispersive spectrometry (WDS) for Fe, Mg, and Ca using a Cameca SX-100 electron microprobe at the RSES, ANU, operating with 15 kV and a beam current of 10 nA and a defocused beam of 5 µm diameter. Natural calcite, dolomite, and magnesite were used as secondary standards.

Powder X-ray diffraction

Powder X-ray diffraction analyses were performed with a Siemens D501 diffractometer, equipped with a curved graphite monochromator and a scintillation detector, using CuKα radiation. An internal standard (silicon, NIST SRM 640c) was added to the samples, which were ground up manually in acetone with an agate mortar, then mounted on a quartz low-background holder, and scanned between 17 and 90° 2θ, at a step width of 0.02° and scan speeds ranging from 0.1° to 0.45°/min depending on sample size.

Crystal structure, ordering parameter, and refinement

Dolomite $CaMg(CO_3)_2$ is a rhombohedral carbonate, and its structure and crystal chemistry are described and discussed by Reeder (1983). Common, natural dolomite is ordered, whereby layers parallel to (001) occupied by Mg atoms only alternate with those occupied with Ca. This ordering pattern gives rise to space group *R-3* and produces

Table 2 Rietveld refinement results for dolomite. Goodness-of-fit values (R_P, R_{wp}, X^2), ordering parameter (S), peak intensity ratio (I_{015}/I_{006}), preferred orientation parameter (PO), concentration of dolomite in the sample (wt%), and other phases present in the sample and included in refinement

Sample	R_P	R_{wp}	χ^2	S	I_{015}/I_{006}	PO	wt %	Other phases
LB	7.68	10.50	5.43	1.00(2)	0.66	0.69(1)	99.5(8)	si, mu, bio
125	10.34	13.73	2.31	0.97(2)	0.82	0.84(1)	74(1)	si, mag, ara, *Pt*, *AgCl*
126	10.06	12.88	3.54	0.86(2)	0.87	1.00(1)	84(1)	si, mag, *Pt*, *AgCl*
127	8.79	12.09	1.76	0.88(2)	0.80	0.84(1)	72(1)	si, mag, ara, *Pt*, *AgCl*
128	11.33	15.43	1.49	0.88(4)	0.83	0.82(1)	67(1)	si, mag, ara, *Pt*
129	10.47	14.05	1.52	0.88(2)	0.76	0.83(1)	74(1)	si, mag, ara, *Pt*
130	11.06	15.50	1.44	0.89(4)	0.72	0.75(1)	38(1)	si, mag, ara, *Pt*, *AgCl*
131	9.71	13.70	2.00	0.89(6)	0.88	0.68(1)	17(1)	si, mag, ara, *Pt*
C-1915	12.44	17.07	2.73	0.95(14)	0.70	0.73(1)	33(1)	si, cc, ara
140	9.89	13.34	1.83	0.92(4)	0.67	0.72(1)	45(1)	si, mag, ara, *Pt*
143	9.05	12.32	1.89	0.96(2)	0.74	0.78(1)	74(1)	si, mag, *Pt*
136	11.10	15.71	2.01	0.80(8)	0.92	0.89(1)	17(1)	si, cc, ara
C-1911	11.73	15.37	1.87	0.88(6)	0.64	0.69(1)	31(1)	si, cc, *Pt*
138	10.04	13.67	2.18	0.90(6)	0.71	0.81(1)	18(1)	si, cc, ara
137	9.23	11.84	3.10	0.85(18)	0.63	0.93(1)	7(1)	si, cc
H152	8.10	10.92	3.45	0.81(2)	0.71	0.89(1)	82(1)	si, *per*
H150	8.78	11.36	3.91	0.75(4)	0.47	0.90(1)	26(1)	si, cc, *Pt*, *per*
H154	11.09	13.57	6.11	0.70(10)	0.66	0.97(1)	19(1)	si, cc, *Pt*, *per*, *hal*
UHP136	14.66	19.29	2.48	0.08(4)	0.43	0.80(1)	74(1)	si, cc, bru, ar, *gr*
UHP 133	13.85	18.49	5.37	0.01(4)	0.00	0.80(1)	25(1)	si, cc, bru
C-3268	12.91	18.79	5.65	0.00(4)	0.00	1.01(1)	49(1)	si, cc, mag, bru

$R_P = \sum |y_{io} - y_{ic}| / \sum y_{io}$ where y_{io} and y_{ic} are observed and calculated intensity at point i

$R_{WP} = \left[\left(\sum W_i (y_{io} - y_{ic}) / \sum W_i y_{io}^2 \right) \right]^{1/2}$, where w_i is the weight assigned to each observation

$\chi^2 = \left[\left(\sum W_i (y_{io} - y_{ic}) \right) / (N - P) \right]^2 = \left[R_{WP} / R_{exp} \right]^2$

$S = 2N - 1$, where N = (number of Ca atoms on A site)/(total number of Ca atoms), error is 2σ

I_{015}/I_{006} = (intensity of reflection 015)/(intensity of reflection 006)

$PO = [P1^2 \cos^2\alpha_k + P1^{-1} \sin^2\alpha_k]^{-3/2}$

LB Lengenbach dolomite starting material. Mineral abbreviations *si* silicon (standard), *mu* muscovite, *bio* biotite, *mag* magnesite, *ara* aragonite, *cc* calcite, *per* periclase, *hal* halite, *bru* brucite, *gr* graphite, *Pt* platinum

Phases in italics are likely small contaminations from the assembly and capsule material

three small but clear ordering reflections (101, 015, and 021) in the X-ray diffraction pattern. Disordered dolomite, in contrast, is characterized by a completely random distribution of Ca and Mg atoms, space group *R-3c*, and the absence of the three ordering peaks; it is isostructural with calcite.

The intensity of the three ordering reflections in the dolomite diffraction pattern can be used to determine the degree of ordering, i.e., the magnitude of ordering parameter *S*. This parameter was defined by Reeder (1983) as $S = 2N - 1$ assuming ideal dolomite composition, with N being the number of Ca atoms on site A [referring to formula $(AB(CO_3)_2]$ divided by the total number of Ca atoms. Thus, fully ordered dolomite has an *S* of 1, whereas fully disordered dolomite has an *S* of 0. In some previous studies (e.g., Luth 2001, Morlidge et al. 2006), dolomite ordering was determined with the Schultz-Güttler (1986) method, which relies on measuring the intensities of only two reflections, and using the I_{015}/I_{006} intensity ratio. Since this method is affected by preferred orientation in the sample, we concur with the studies by Antao et al. (2004) and Hammouda et al. (2011) that Rietveld structure refinement is a more reliable method for modeling order in dolomite, as it uses all of the peaks in the diffraction pattern, and can even account to a certain extent for preferred orientation. Our data obtained with the Schultz-Güttler (1986) method I_{015}/I_{006} are also presented here (Table 2), but they display very large scatter and are not used for interpretation.

Crystal structure refinement was carried out with the Rietveld method, using the computer program RIETICA 2.1 (Hunter 1998). All crystalline phases that were identified with SEM or XRD were included in the refinement. Refined parameters include up to six background parameters, zero correction, asymmetry parameter, scale parameters of all phases, up to six peak shape parameters per phase, and one preferred orientation parameter per phase

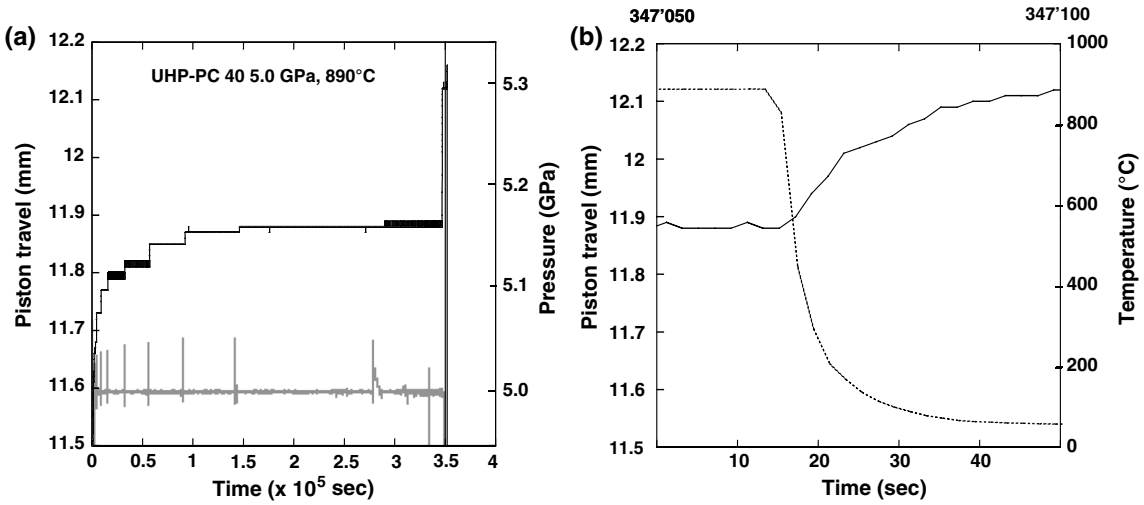

Fig. 2 **a** Piston travel (*black line*) and nominal pressure (*gray line*) during a 96-h run at 5 GPa logged by the automated UHP piston cylinder. Steady-state conditions were reached after about 1 day. *Spikes* in the pressure curve are related to automatic oil pressure strikes in order to maintain the nominal pressure of 5 GPa. **b** Detail of the log data during quenching. The temperature (*dashed line*) drops to <200 °C in less than 10 s. The piston moves in due to thermal compaction of the assembly

where appropriate. Unit cell dimensions of all major phases were refined except for the internal standard silicon. Starting parameters for dolomite were taken from Reeder (1983, Lake Arthur sample). The occupancy factors for the two cation sites were constrained to full occupation with either Ca or Mg, and a composition of ideal dolomite $CaMg(CO_3)_2$. Rietveld refinement of dolomite in some experimental samples was a challenge because of small sample sizes (<1 mm^3), and due to the fact that the phase of interest occurred with up to five other phases, and was often present only as a minor component (Table 2), resulting in very low peak intensities. Moreover, some of the samples contained Mg-rich calcite, causing significant peak overlap with dolomite. This limits the quality of the data available for refinement and thus, the number of parameters that could be refined for dolomite. For example, it was not possible to refine for every sample the atom coordinates *x*, *y*, *z* as well as atomic displacement parameters *B* for dolomite. The oxygen position was commonly unstable, and the displacement parameters correlated strongly with occupancy factors, sometimes resulting in unrealistic, negative *B* values. Thus, the atom coordinates *x*, *y*, *z* as well as atomic displacement parameters *B* were fixed to the values of Reeder (1983, Lake Arthur sample) in the refinements of samples 130, 131, UHP 133, 136, UHP 136, 137, 138, 150, 154, C-1911, C-3268. The limitations of the XRD data for dolomite explain the relatively large R-factors of the refinements (Table 2).

Preferred orientation of dolomite in some of the XRD specimens is significant due to the excellent cleavage along the (104) plane (Table 2), with preferred orientation parameters (PO) ranging from 0.69 to 1.01. A randomly oriented sample has a preferred orientation parameter (PO) of 1, whereas PO < 1 and PO > 1 indicate preferred orientation for plate-like and needle-shaped crystals, respectively. In carefully prepared XRD samples that are large enough to allow predominantly grain support within the sample, the PO is typically between 0.9 and 1.1. If samples are very small so that a large proportion of the crystals rest directly on the flat surface of the sample holder, as in this study, preferred orientation can increase to more extreme values like 0.69 in our sample C-1911. The physical effect of PO = 0.69, for example, is to increase the intensity of the 104 reflection by 42 %, thus decreasing the relative intensities of all other reflections, which makes the determination of subtle intensity changes that are due to cation ordering impossible, unless preferred orientation is included in the refinement model. The preferred orientation models available however allow for only one preferred orientation direction and cannot cater for samples where preferred orientation may occur on other directions as well, which is most likely the case in most samples. We tested the effect that preferred orientation in the XRD specimens has on the ordering parameter. For this purpose, one Lengenbach sample was prepared on a thin film. Apart from being analyzed in reflection geometry like all other samples, it was also analyzed with a second diffractometer on a transmission stage (STOE Stadi-P), thus reversing the preferred orientation effect (not shown here). The resulting preferred orientation parameters were 0.72 and 1.13, respectively. The corresponding ordering parameters *S* varied from 0.94 to 1, so that the error in *S* that is associated with specimen preparation, in particular preferred orientation, was estimated to be no larger than ±0.06.

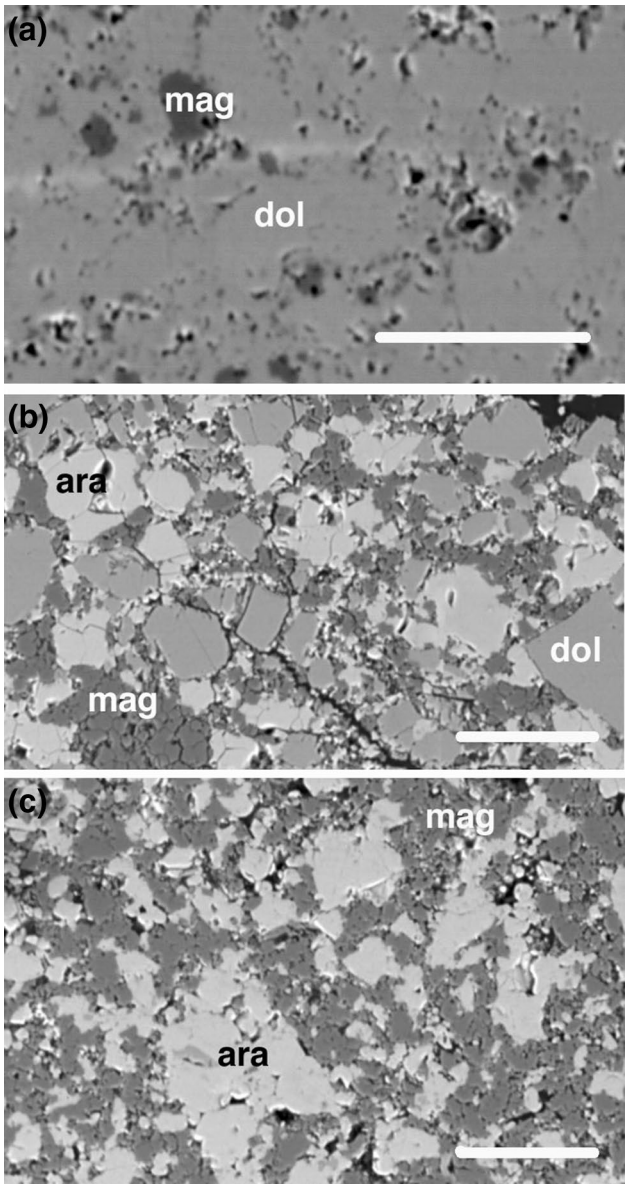

Fig. 3 Backscatter electron (BSE) images of run products from the investigation of the reaction dolomite -> aragonite + magnesite at 650 °C. **a** Formation of dolomite with minor residual magnesite (5.1 GPa). **b** No reaction between the three carbonates is observed (5.6 GPa). **c** Complete disappearance of dolomite and equilibrium textures of magnesite and aragonite (5.8 GPa). *Scale bar* is 20 µm

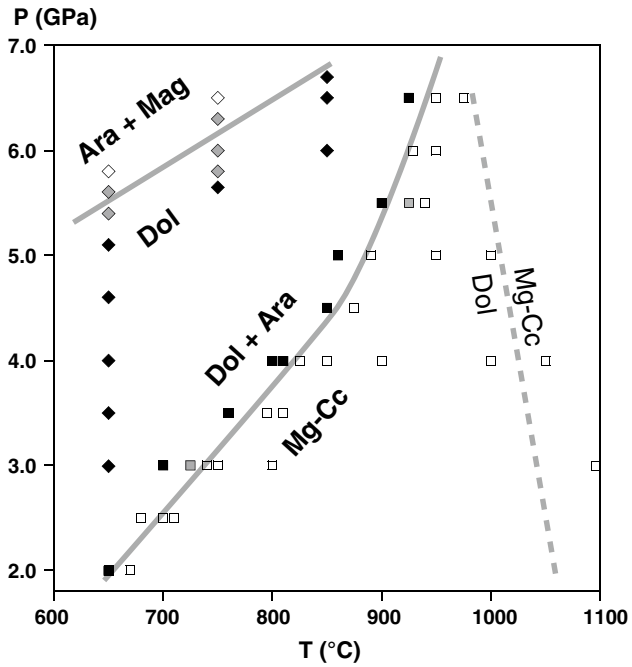

Fig. 4 *P–T* grid with performed experiments. *Diamonds* relate to experiments to constrain the reaction dolomite = aragonite + magnesite. *Black filled symbols* dolomite growth; *gray filled symbols* no reaction; *open symbols* aragonite and magnesite growth. *Squares* are for the reaction aragonite + dolomite = Mg-calcite. *Black filled symbols* dolomite + aragonite; *gray filled symbols* unclear relations; *open symbols* Mg-calcite forms

Results

Phase relations

The results of experiments are summarized in Table 1. Typical textures related to the investigation of the reaction Dol = Ara + Mag are shown in Fig. 3. At 650 °C, the formation of dolomite at the expense of Ara + Mag is run to near completion up to pressures of 5.1 GPa, producing more than 95 % dolomite and leaving only isolated islands of magnesite and rare aragonite (Fig. 3a). At 5.4 and 5.6 GPa, no reaction was observed, and all three carbonates appear as in the starting material (Fig. 3b). This is quite surprising as a CO_2–H_2O fluid acting as a flux has been used to promote reaction in these experiments. Dolomite disappears at 5.8 GPa, and aragonite + magnesite is stable (Fig. 3c). At 750 °C, dolomite was found up to a pressure of 5.7 GPa, whereas no reaction took place at 5.8–6.3 GPa. Aragonite + magnesite occurred at 6.5 GPa. At 850 °C, dolomite was present up to the highest possible pressure reached of 6.7 GPa. These observations provide evidence that the reaction Dol = Ara + Mag has a positive slope in the 650–850 °C temperature range (Fig. 4).

The reaction Dol + Ara = Mg-Cc was investigated in the pressure range from 2 to 6.5 GPa in 0.5 GPa steps (Fig. 4). The observed changes in textures are illustrated in an isobaric *T–X* section at 4 GPa (Fig. 5). Aragonite and dolomite coexist up to 810 °C and display a tight intergrowth throughout the capsule. Mg-calcite first appears in the run at 825 °C with a *X*(Ca) of 0.8. The experiment produced significantly more Mg-calcite than dolomite, and aragonite has completely reacted away, in agreement with the expected proportions for a bulk of *X*(Ca) of 0.74 in the starting material. At 850 °C, for the same starting material,

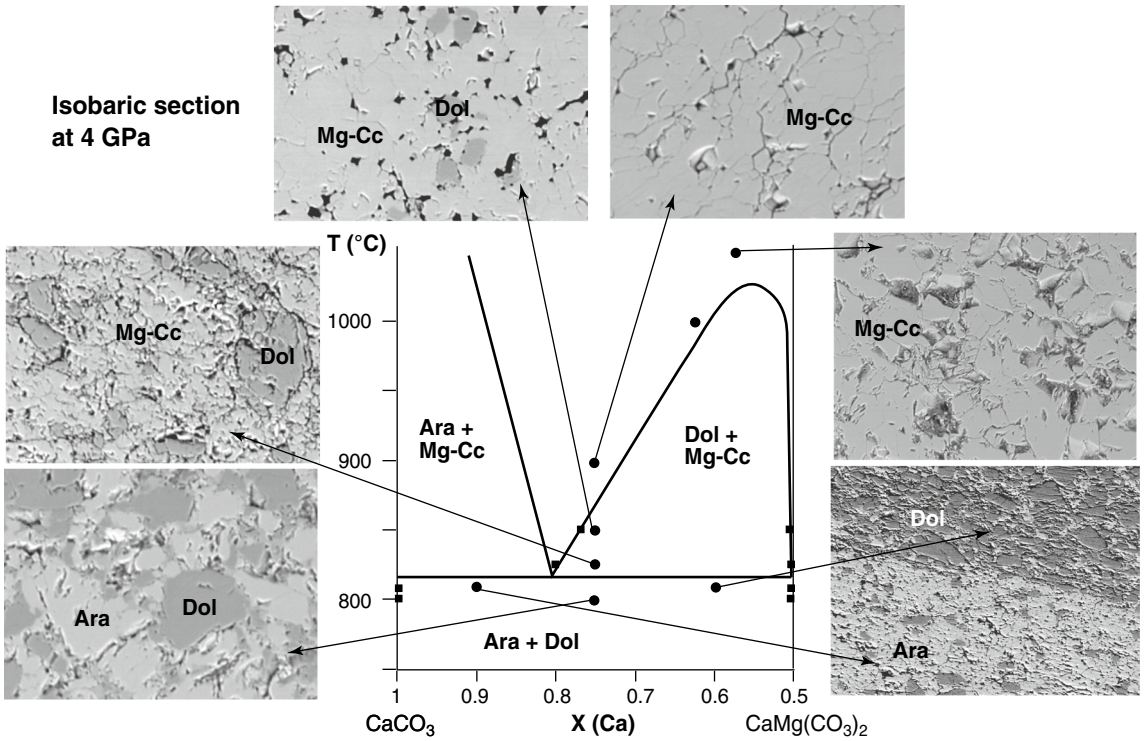

Fig. 5 Temperature (°C)—composition section at 4 GPa with typical textures of experimental runs. *Filled circles* show the bulk composition used in the experiments, and *filled squares* show the composition of the phases after the experiment. The *lower right image* comes from experiment UHP 49 where a layered starting material (Mix 4) was used

the amount of dolomite decreases further as the composition of Mg-calcite moves to lower X(Ca). At 900 °C, a single, unbuffered Mg-calcite is present with the composition of the starting mix. In order to constrain the solvus to higher temperatures, additional experiments were run with a more Mg-rich starting material. In the resulting T–X section, neither the reaction Dol = Ara + Mag nor the reaction Dol = Mg-Cc + Mag are crossed, and thus, this represents a section through the phase diagram at a lower pressure than what is schematically shown in Fig. 1b. As the main aim of this paper is to investigate the reaction Dol + Ara = Mg-Cc, most of the experiments have been conducted close to the reaction boundary. The experimental results show that this reaction steepens up with increasing pressure (Fig. 4).

Phase compositions

The composition of the analyzed carbonates is given in Table 1. Aragonite is pure and does not contain detectable amounts of MgO (<0.03 wt%). Magnesite coexistent with aragonite has only been produced in a few experiment and contains a X(Ca) of 0.02 at 650 °C and 0.03 at 750 °C. At 1100 °C, 3 GPa, minor magnesite with a higher X(Ca) of 0.07 coexisted with dolomite. Dolomite is close to the stoichiometric value of X(Ca) = 0.5 apart from an experiment at 975 °C, 6.5 GPa where it has clearly higher X(Ca) of 0.53. As expected, the Mg-calcite covers a wide range of compositions (Fig. 6a). The highest X(Ca) = 0.89 has been found where the Mg-calcite formed at the lowest pressure/temperature, i.e., at 2 GPa, 670 °C. The composition of Mg-calcite that first appears on the reaction curve is independent of whether aragonite or dolomite coexists (Fig. 1). The composition of Mg-calcite [X(Ca) = 0.89] coexisting with aragonite approaches the Mg-calcite [X(Ca) = 0.87] coexisting with dolomite at 700 °C, 2.5 GPa. Thus, the composition of Mg-Cc at the reaction curve at 2.5 GPa is constrained to 0.88 (Fig. 6b). The experiment at 2.5 GPa, 680 °C is interpreted as an outlier in the composition as it has too high an X(Ca). Indeed, this sample does also not fit very well the overall determined reaction boundary, and thus, this experiment should be treated with caution. The first appearance of Mg-calcite increases in temperature with increasing pressure, and concomitantly, the Mg-calcite coexisting with dolomite gets richer in MgO, in agreement with the theoretical considerations (Fig. 1). The polybaric projections of all Mg-calcite compositions approximately follow a solvus (Fig. 6a). However, detailed inspection shows that the solvus tends to shrink with increasing pressure. The best constraint on the crest of the solvus is

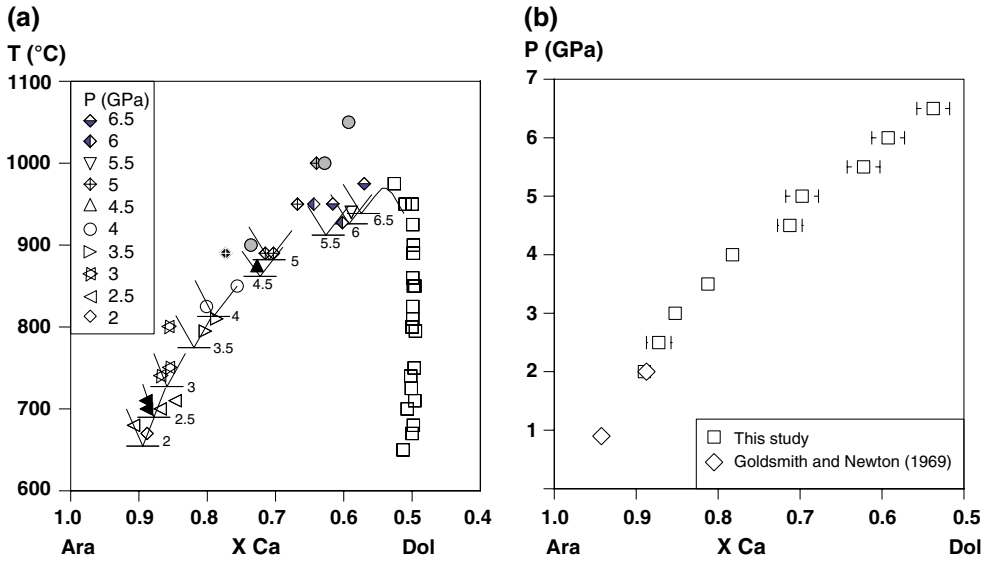

Fig. 6 **a** Composition of dolomite (*squares*) and Mg-calcite (*other symbols*) in the experiments as a function of temperature and pressure. The *lines mark* the position of the minimum temperature and composition of Mg-calcite as shown in Fig. 5. *Different symbols* are used for the different pressures. *Empty symbols* coexisting with dolomite; *gray filled symbols* single-phase carbonate; *black filled symbols* coexisting with aragonite. The closure of the solvus between Mg-calcite and dolomite is nearly reached at 6.5 GPa, 975 °C run. **b** The composition of Mg-Calcite along the univariant reaction aragonite + dolomite = Mg-calcite as a function of pressure. *Squares* are from this study, and *diamonds* are from Goldsmith and Newton (1969)

given by the experiment at 6.5 GPa, 975 °C with a starting material of $X(\mathrm{Ca}) = 0.55$, where the Mg-calcite (0.57) and dolomite composition (0.53) is very close, indicating that the solvus likely closes at ~1000 °C. From the observation that the solvus slightly shrinks with increasing pressure, it is deduced that the critical curve Dol = Mg-Cc must have a slight negative slope in *P–T* space (Fig. 4). As dictated by the phase rule, the composition of the Mg-calcite along the univariant reaction curve changes steadily as a function of pressure (Fig. 6b).

X-ray diffraction and dolomite ordering

XRD results for all dolomite-bearing samples are summarized in Table 2. Four different carbonates were identified in the samples (aragonite, calcite, dolomite, magnesite), as well as small amounts of periclase, brucite, and graphite. The presence of platinum, silver chloride, and halite in many experimental samples represents contamination with components from the high-pressure assembly that happened during sample recovery. Traces of muscovite and biotite were present in the natural sample from Lengenbach, while silicon occurred in all samples as the internal standard.

The state of order of Ca and Mg in the dolomite structure is represented by the ordering parameter *S* (Reeder and Wenk 1983) that was determined with full profile Rietveld refinement (Table 2). An example of such a refinement is shown in Fig. 7a. All degrees of order were encountered in the samples presented here, from complete order in the Lengenbach dolomite sample with pronounced ordering peaks 101, 015, and 021 (Fig. 8a), to complete disorder in sample C-3268 that was equilibrated at the highest temperature (1100 °C; Fig. 8b). All measured dolomites follow a general trend. Figure 7b shows that the starting material, which formed at 450 °C and cooled slowly during retrograde metamorphism, is fully ordered ($S = 1$). At the lowest experimental temperature of 650 °C, the dolomites display a small degree of disorder with *S* values between 0.97 and 0.9. With increasing temperature up to 950 °C, there is a gradual decrease in *S* values to 0.7. The most striking feature is observed between the experiment at 950 °C, 6 GPa and 975 °C, 6.5 GPa, where *S* drops from 0.7 to 0.08. Dolomites at higher temperatures are fully disordered. A weak trend of ordering with pressure is seen in that the transition from highly ordered to weakly ordered dolomite shifts to slightly lower temperatures with increasing pressure. Since the X-ray diffraction analyses were carried out on quenched samples, and not in situ, it is possible that some ordering might take place during cooling (Reeder and Wenk 1983), and that the state of order at run conditions was lower than the one reported here. However, given that complete disorder was retained in the hottest sample, the effect of ordering during our fast quenching (Fig. 2b) seems to be minimal.

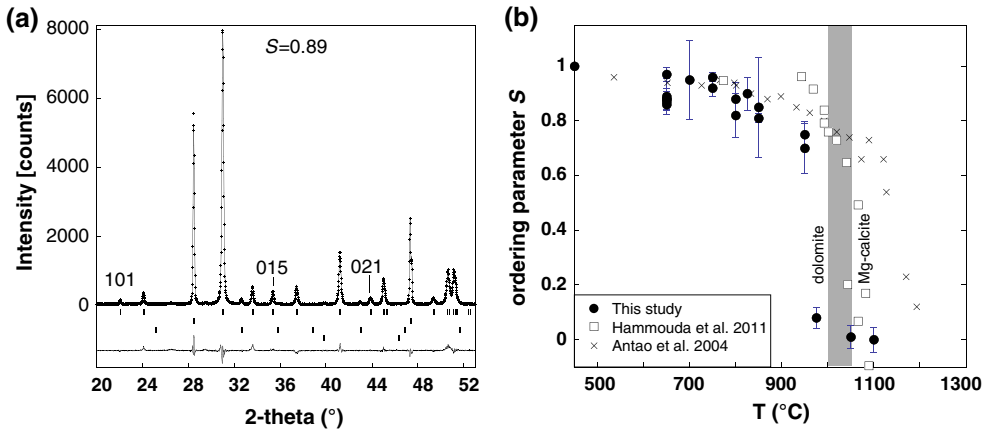

Fig. 7 **a** Example of Rietveld refinement result (sample 130) for the determination of the order parameter *S*. The presence of reflections 101, 015, and 021 indicates a certain degree of order of Ca and Mg atoms in the crystal structure with $S = 0.89(1)$. Crosses: observed pattern, *upper solid line* calculated pattern, *vertical bars* peak positions for dolomite, silicon, magnesite, and platinum (from *top* to *bottom*), *lower solid line* difference pattern. **b** Order parameter *S* of dolomite determined with Rietveld refinement (*solid circles*) compared to in situ analyses from the study of Antao et al. (2004) conducted at 3 GPa (crosses) and of Hammouda et al. (2011) conducted at 3.4–4 GPa (*open squares*). The *gray* band corresponds to the estimated temperature for the closure of the solvus between dolomite and Mg-calcite in the range 3–6 GPa (Fig. 4)

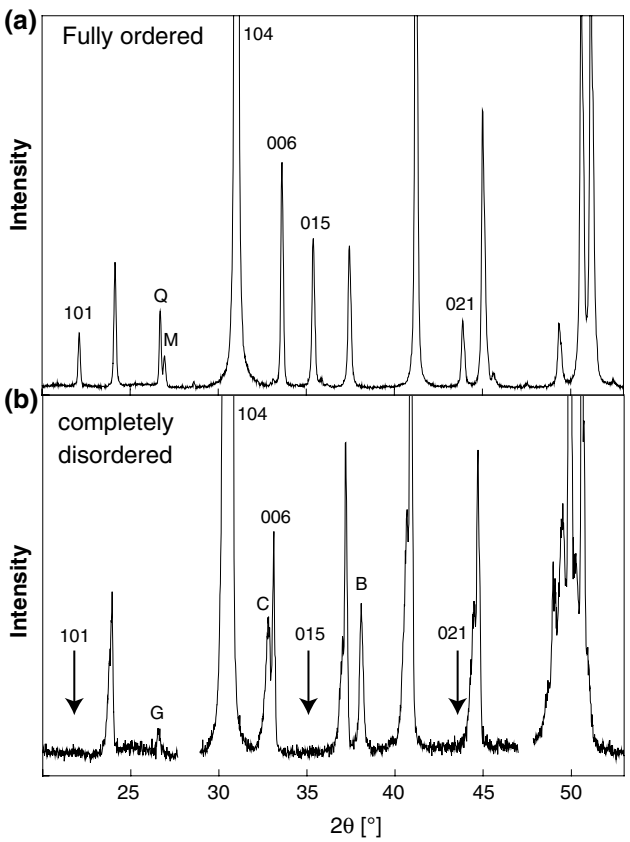

Fig. 8 Detail of X-ray diffraction patterns of fully ordered and disordered dolomite. **a** Lengenbach dolomite. **b** Sample UHP 133. Note the absence of ordering reflections 101, 015, and 021. Peaks of contaminating phases are labeled Q (quartz), M (mica), and G (graphite)

The unit cell dimensions of Mg-calcite in our samples are notably smaller than the ones of previous high-pressure, high-temperature studies (Bischoff et al. 1983; Goldsmith et al. 1961), with *a* and *c* differing by up to 0.4 %, resulting in unit cell volumes that are up to 1 % smaller (e.g., our calcite with 12.5 mol % $MgCO_3$ (sample C-1911) and $a = 4.9212(2)$ Å, $c = 16.7440(9)$ Å), $V = 351.18$ Å compared to sample 7C of Bischoff et al. (1983) with 13 mol % $MgCO_3$ with the dimensions $a = 4.9336(7)$ Å, $c = 16.806(5)$ Å), $V = 354.3(1)$ Å). The smaller Mg-calcite volumes of this study are consistent with the significantly higher experimental pressures (2–6.5 GPa) compared to those used in the above previous studies (<1.5 GPa). It could be speculated that the Mg-calcite structure adjusts to higher pressures by the formation of local domains characterized by Ca–Mg short-range order, explaining the decrease in overall volume without formation of ordering peaks in XRD patterns.

Discussion

Approach to equilibrium

The reaction Dol + Ara = Mg-Cc produced nicely equilibrated textures (Fig. 5). The reaction was bracketed in a 20–25 °C interval, and generally no relict phases were observed, indicating that during the long durations of the experiments, the reaction went to completion. The reaction is univariant, and thus, the composition of Mg-Cc should change systematically along the reaction curve as

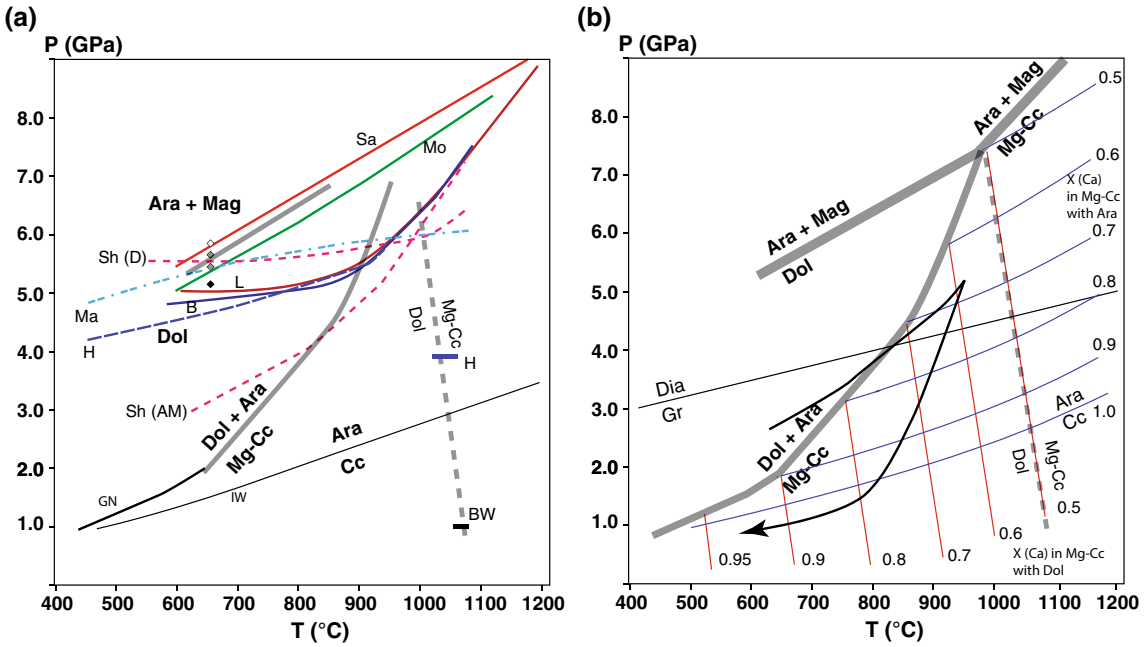

Fig. 9 **a** Compilation of experimental results for the $CaCO_3$–$CaMg(CO_3)_2$ system. *Bold gray lines* are from this study (piston cylinder). Other piston cylinder studies: *GN* Goldsmith and Newton (1969), *IW* Irving and Wyllie (1975), *BW* Byrnes and Wyllie (1981). Multi-anvil studies on quenched samples *L* Luth (2001), *S* Sato and Katsura (2001), *M* Morlidge et al. (2006), *B* Buob et al. (2006). In situ studies: *Ma* Martinez et al. (1996); *Sh* Shirasaka et al. (2002) with (D) labeling the "dolomite out" and (AM) the "aragonite + magnesite in" curve; *H* Hammouda et al. (2011). **b** Petrogenetic grid based on the experimental results. Graphite–diamond phase boundary after Bundy et al. (1961). Compositional isopleths for Mg-calcite coexistent with aragonite (*blue line*) or dolomite (*red lines*) are given as *X*(Ca). A general *P*–*T* path of the Kokchetav UHP rocks (Hermann et al. 2001) is shown with a *black line* and *arrow*

a function of pressure/temperature. Indeed, there is a very smooth trend in the composition of Mg-Cc along the reaction (Fig. 6b). All these observations indicate that equilibrium has been attained in this set of experiments.

In contrast, Dol = Ara + Mag is sluggish, and the reaction has to be overstepped significantly in order to drive the reaction to completion. Such difficulties in reaction kinetics have been noted also in previous studies, where metastable phases have been observed (Luth 2001; Shirasaka et al. 2002). We have used a starting material that consists of all three phases in order to bracket the reaction. To promote reaction, we have added oxalic acid dihydrate that produces a CO_2–H_2O fluid at run conditions and acts as a flux. As the reaction is univariant, the addition of a fluid phase does not have an influence on the position of the reaction. The run duration in our experiments ranged from 72 to 168 h to give enough time for equilibration. Apart from the study of Buob et al. (2006), which used similarly long-run durations, all previous experiments used much shorter run times of 24 h with a few experiments running for 48 h. Even with our long-run times and a fluid phase to flux the reaction, there is a 0.5-GPa interval at 650 and 750 °C, where all three carbonates are present.

Despite differences in the position of the Dol = Ara + Mag reactions at intermediate temperature (see next section), all studies report the reaction at very similar pressure at 600–650 °C. This provides an excellent opportunity to cross-calibrate pressures obtained by multi-anvil studies using quench technique as well as in situ X-ray analysis with our UHP piston cylinder technique at low temperature. The bracket obtained at 650 °C is in good agreement with the in situ synchrotron X-ray analyses of Martinez et al. (1996) and the reaction curves determined by Sato and Katsura (2001) and Morlidge et al. (2006), but at slightly higher pressures than the curves of Luth (2001), Buob et al. (2006) and Hammouda et al. (2011; Fig. 9a). This provides evidence that no significant friction builds up in the low friction assemblies used, and the measurement of piston travel (Fig. 2) during long-run durations permits us to monitor when friction decay is close to completion. Also the movement of the piston after quenching of the experiment indicates that no jamming of the piston due to bulging occurred. The calibration bracket has been obtained at the lowest temperature investigated, and it is expected that friction is similar or smaller at the higher run temperatures.

Comparison with previous studies

The reaction Ara + Dol = Mg-Cc has been investigated by Goldsmith and Newton (1969) up to 2.2 GPa. There is

excellent agreement with our study on the position of the reaction curve at 2 GPa (Fig. 9a), and the compositions of Mg-calcite on the reaction curve at 2 GPa are within error the same (Fig. 6b). Moreover, the slight shrinking of the Dol = Mg-Cc solvus with pressure documented here from 2.5 to 6 GPa has also been observed by Goldschmidt and Newton at 0.1–2 GPa. The combined results thus show a trend of a gradual steepening of the reaction with increasing pressure that can be attributed to the increased incorporation of Mg into Mg-Cc. Within the pressure range of this study, the termination of the reaction Ara + Dol = Mg-Cc has not been reached. At 6.5 GPa, 975 °C, dolomite coexists with Mg-calcite, and at 6.7 GPa, 850 °C, dolomite is present, indicating that the invariant point (Fig. 1) is situated at higher pressures. The slope of the critical curve can be constrained by several observations. The opening of the solvus with decreasing pressure suggests that the critical curve is located at slightly higher T at lower pressure, resulting in a slight negative slope, in agreement with the phase analysis of Irving and Wyllie (1975). At 4 GPa, 1050 °C, we observed a fully disordered dolomite (Table 2), indicating that the solvus has been crossed. This is in good agreement with the in situ data of Hammouda et al. (2011) who reported the transition from ordered to disordered dolomite at 1030–1070 °C at 3.4–4 GPa (Fig. 7). The experiments of Byrnes and Wyllie (1981) placed the closure of the solvus at ~1080 °C at 1 GPa (Fig. 9) providing further evidence for a negative slope of the critical curve Dol = Mg-Cc.

The reaction Dol = Ara + Mag has been studied experimentally by various groups in the last 20 years using different techniques, and the results scatter significantly (Fig. 9a). The first study of this reaction was by in situ X-ray diffraction of experiments using a DIA-type cubic anvil apparatus (Martinez et al. 1996). These authors reported the first appearance of Ara + Mag from a dolomite starting material at 5.5 GPa at 600 °C. In situ synchrotron X-ray diffraction multi-anvil experiments by Shirasaka et al. (2002) showed an enormous gap between the breakdown reaction of dolomite to Ara + Mag with respect to the synthesis of dolomite from Ara + Mag (Fig. 8a). These authors argued that the initiation of the breakdown of dolomite should be used as the reaction boundary. However, it is important to note that none of the relatively short experiments (<2.5 h) produced a dolomite-free Ara + Mag assemblage. Hammouda et al. (2011) used a similar approach as Shirasaka et al. (2002) and constrained three points on the Dol = Ara + Mag curve with a Fe-bearing dolomite as starting material (7 mol % $FeCO_3$). Their reaction curve has a similar slope to the proposed curve of Martinez, but is placed at lower pressures (Fig. 9a). Steep reaction curves are reported by Sato and Katsura (2001) and Morlidge et al. (2006) using quench techniques in a multi-anvil apparatus. Using the same technique, Luth (2001) and Buob et al. (2006) found nearly flat reaction curves that steepen up at 900 °C. At this temperature, the difference in the position of the reaction is ~2 GPa with respect to Sato and Katsura (2001) and Morlidge et al. (2006), far above the given uncertainty in the pressure of multi-anvil experiments. Buob et al. (2006) used a starting material containing all three phases, as in our study, and thus reversed the reaction. While Luth (2001) reported metastable dolomite far into the Ara + Mag field, no metastable dolomite was found by Buob et al. (2006). Our study in defining the location of the Dol = Ara + Mag is restricted by the upper pressure range of the UHP piston cylinder to 6.7 GPa. Our data are in excellent agreement with Sato and Katsura (2001) and Morlidge et al. (2006), and inconsistent with the curves of Luth (2001) and Buob et al. (2006). Potential discrepancies between the two sets of reaction curves have been discussed in detail by Morlidge et al. (2006). They argued that order–disorder in dolomite and reaction kinetics are potential sources for disagreement. However, Hammouda et al. (2011) measured the degree of disorder in dolomite in situ, and their reaction curve is again different. While there is some disorder in the dolomite measured in our experiments (see next section), it cannot account for the big difference in the position of the reaction curve and the reasons for the discrepancies remain unclear.

Order–disorder in carbonates

The highest degree of order with $S = 1$ was found in the natural Lengenbach dolomite, the crystal structure of which should represent the ideal ordered state as it was equilibrated at around 450 °C and cooled slowly in a regional metamorphic setting. A significant decrease in S was observed between 850 and 950 °C, with the most dramatic drop off observed between 950 and 975 °C (Fig. 7b). The sample equilibrated at 1100 °C does not show any ordering reflections in the XRD trace, with a corresponding S value of 0.0. The sharp drop off corresponds in temperature with the closure of the calcite–dolomite solvus (Fig. 7b). Thus, we note that rather than using the commonly used term "disordered dolomite," some might find it more appropriate to call this phase "Mg-calcite with X(Ca) of 0.5." The X-ray diffraction work was carried out on samples that quenched in a short time of less than 20 s (Fig. 2b). Nevertheless, it has to be evaluated whether ordering in dolomite occurred during cooling (Reeder and Wenk 1983). We observe full disorder in an experiment with X(Ca) of 0.5 that was run at the highest temperature of 1100 °C. This is in agreement with the data of Luth (2001) and Morlidge et al. (2006) on quenched carbonates who found completely disordered carbonate (probably Mg-Cc with X(Ca) of 0.5) in experiments at temperatures above 1050 °C. Our data can also be compared with in situ studies of ordering

in carbonates. The study of Hammouda et al. (2011) found that complete disorder was attained at 1070 (±20) °C for pressures between 3.4 and 4 GPa. Then, S increased from ~0.6 to close to 1, and no significant disorder at temperatures below 900 °C was observed. In the temperature range of 650–1050 °C, our data points follow more closely the 3 GPa in situ measurements of Antao et al. (2004) showing a gradual increase in disorder over a temperature interval of about 300–400 °C. This latter study found complete disorder at higher temperature than in our study, which might be related to the difficulties in obtaining exact absolute temperatures in the in situ experiments.

Since the first detailed study of quenched samples on the reaction Dol = Ara + Mag by Luth (2001), it has been speculated to what extent order–disorder in dolomite will affect the position and slope of the reaction. For example, Luth suggested that the increasing disorder of dolomite expands the dolomite stability field to higher pressures resulting in a steepening of the reaction curve. Our compilation shows that the transition from ordered to disordered dolomite coincides with the critical curve Dol = Mg-Cc (Fig. 7), which is situated at about 100 °C higher temperatures than the inflection of the reaction proposed by Luth (2001). On the other hand, Hammouda et al. (2011) suggested that disorder of dolomite should shift the reaction to lower pressures and that the steep reaction of Morlidge et al. (2006) represents the reaction boundary for fully ordered dolomite. The reaction determined in this study agrees very well with the study of Morlidge et al. (2006); yet, we observe a systematic increase in disorder of dolomite with increasing temperature. Thus, it seems unlikely that variable degrees of disorder are responsible for the different positions of the Dol = Ara + Mag reaction (Fig. 9).

Petrogenetic grid for carbonates along the aragonite–dolomite join

Our study differs from previous work in that it aims to take all possible reactions into consideration (Fig. 1). The influence of the reaction Ara + Dol = Mg-Cc and the closure of the solvus Dol = Mg-Cc on the reaction Dol = Ara + Mag have not been explored so far. Phase relations dictate that the Dol = Ara + Mag reaction must terminate at an invariant point and is followed by the reaction Ara + Mag = Mg-Cc (Fig. 1). This invariant point represents the uppermost pressure stability of dolomite, whereas the maximum temperature stability is given by the critical curve, which is situated at $T < 1050$ °C at pressures above 5 GPa. Although the exact location of the invariant point was at pressures beyond the capability of the UHP piston cylinder, we have good constraints to place it approximately at ~7.5 GPa, ~1000 °C (Fig. 9b). This implies that high-pressure experiments reported in the literature at $T \geq 1050$ °C are unlikely to constrain the Dol = Ara + Mag reaction. It is an unfortunate coincidence that most experiments run at 6.5–9 GPa and 1000–1200 °C used a bulk starting material with X(Ca) ~0.5, which in most cases produces a single-phase, unbuffered carbonate (e.g., Figure 1b). XRD analyses of carbonates by Luth (2001) show fully disordered "dolomite" at these conditions, which is consistent with Mg-calcite having a X(Ca) of 0.5. Also the "dolomite" in the 1100 °C, 8 GPa experiment of Morlidge et al. (2006) is fully disordered. Therefore, these experiments more likely constrain the dolomite absent reaction Ara + Mag = Mg-Cc at pressures and temperatures above the invariant point. The slope of Ara + Mag = Mg-Cc is constrained by Schreinemakers rule and must be steeper than Dol = Ara + Mag, but flatter than Ara + Dol = Mg-Cc (Fig. 1). It is interesting to note that the inflection in slope of the dolomite breakdown observed by Luth (2001) and Buob et al. (2006) occurs exactly where their low-temperature branch of Dol = Ara + Mag intersects the Ara + Dol = Mg-Cc determined in this study (Fig. 9a). Therefore, it is likely that the steep, high-temperature branch is related to the reaction Ara + Mag = Mg-Cc. The slope of this reaction satisfies Schreinemakers rule with the "steeper" as well as the "flatter" Dol = Ara + Mag reactions (Fig. 9a).

The X(Ca) of Mg-calcite along the reaction Ara + Dol = Mg-Cc changes systematically from 0.9 at 2 GPa to 0.55 at 6.5 GPa. This provides anchor points for compositional isopleths in the system aragonite, Mg-calcite, and dolomite. When coexisting with dolomite, the X(Ca) of Mg-calcite is essentially a thermometer, even at elevated pressures (Goldsmith and Newton 1969). Our study confirms the conclusion of this earlier study that the solvus is slightly shrinking with increasing pressure (Fig. 6a), leading to a small negative slope of the isopleths. In the pure $CaCO_3$ system, the univariant reaction of aragonite to calcite has been determined experimentally (Irving and Wyllie 1975). The addition of Mg into the simple system leads to the transition from a univariant reaction to a divariant field, in which the compositions of the phases are dependent on pressure and temperature. As Mg is only incorporated in calcite, the reduction in the activity of $CaCO_3$ in calcite results in an expansion of the calcite field to higher pressures. Thus, the X(Ca) isopleths should be roughly parallel to the aragonite–calcite reaction in the pure system (Ogasawara et al. 1998). The X(Ca) of Mg-calcite on the reaction Ara + Dol = Mg-Cc is independent of whether it coexists with aragonite or dolomite (Fig. 5), providing anchor points to draw the X(Ca) of Mg-calcite coexisting with aragonite (Fig. 9b).

Application to UHP marbles

The findings of this study have implications for deeply subducted carbonates. Marbles are an important rock type in UHP terrains (Becker and Altherr 1992; Castelli et al. 2007; Sobolev and Shatsky 1990). The breakdown reaction of dolomite to aragonite + magnesite has received a lot of attention as a potential indicator of extreme pressures in UHP terrains (Proyer et al. 2013; Zhang et al. 2003). Some of the most spectacular UHP carbonates occur in the Kokchetav massif, where diamond-bearing marbles have been described in detail (Korsakov and Hermann 2006; Ogasawara et al. 2000; Shatsky et al. 1995). Nanometric inclusions of aragonite and magnesite within diamond from a dolomitic marble are so far the best evidence for a potential coexistence of these minerals in the Kokchetav carbonates (Dobrzhinetskaya et al. 2006). However, if dolomite breakdown was a pervasive feature in dolomitic marbles, abundant magnesite and aragonite inclusions should occur also in peak garnet and clinopyroxene, which is not the case. For this reason, Ogasawara et al. (2000) concluded that peak pressures did not exceed the dolomite stability field. According to our experiments, this would place an absolute upper pressure limit of 7.5 GPa for the UHP metamorphism. Indeed, recent estimations for peak pressures of diamond-bearing gneisses based on inclusions in zircon yield values of 4.9 ± 0.4 GPa (Stepanov et al. 2016). Thus, the question of whether peak metamorphic conditions in the Kokchetav massif were within the Ara + Mag field remains unanswered.

The reaction Dol + Ara = Mg-Cc has received much less attention in studies of UHP carbonates. Ogasawara et al. (2000) were the first to point out that this reaction is important for the interpretation of Mg-calcite in marbles of the Kokchetav massif. These authors showed various textures of Mg-calcite intergrown with dolomite and interpreted them to be the products of the Dol + Ara = Mg-Cc reaction. In the absence of experimental data above 2.2 GPa, they extrapolated the reaction Dol + Ara = Mg-Cc of Goldsmith and Newton (1969) along a constant slope, and consequently, the reaction could only be crossed during the near isothermal decompression from diamond-facies conditions to crustal pressures. Our new experimental determination of this reaction now suggests that Mg-calcite is formed during the prograde evolution (Fig. 9b) of the Kokchetav rocks. Ogasawara et al. (2000) reported the most Mg-rich calcite with $X(\mathrm{Ca}) = 0.78$ from an inclusion in diopside, whereas Shatsky et al. (1995) found a Mg-calcite with an $X(\mathrm{Ca}) = 0.76$ as inclusion in garnet from the Kokchetav marbles. Figure 10 displays an inclusion of a mixed dolomite [$X(\mathrm{Ca}) = 0.51$]–Mg-calcite [$X(\mathrm{Ca}) = 0.88$] inclusion in a garnet found in a garnet–clinopyroxene–dolomite marble

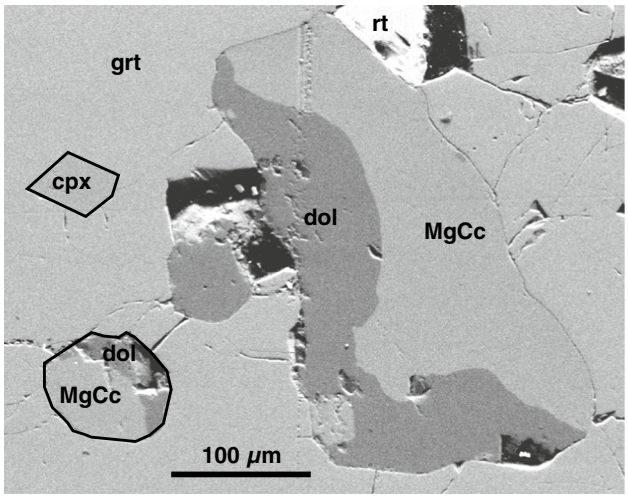

Fig. 10 Backscatter electron image of composite dolomite + Mg-calcite inclusions in garnet from a dolomitic marble from the Kokchetav Massif, Kazakhstan. The inclusions are interpreted to have formed from exsolution of a single carbonate phase trapped during the prograde metamorphism. Abbreviations: *MgCc* Mg-calcite, *dol* dolomite, *cpx* clinopyroxene, *rt* rutile, *grt* garnet

from the Kokchetav massif. Mg-calcite exclusively occurs as inclusion in garnet and clinopyroxene and is always associated with 20–40 % dolomite, suggesting that these composite inclusions originate from unmixing of a more Mg-rich precursor Mg-calcite. A rough estimate of the proportions of dolomite and Mg-calcite suggests that the original single-phase Mg-calcite had a $X(\mathrm{Ca})$ ~0.73–0.8. Figure 9b shows a tentative *P–T* path of the Kokchetav rocks (Hermann et al. 2001) in relation to the carbonate phase relations determined in this study. The reaction Dol + Ara = Mg-Cc is crossed at $X(\mathrm{Ca})$ ~0.75 in good agreement with the estimated composition of Mg-calcite trapped in garnet and diopside. Some of these inclusions occur together with diamond, providing evidence that the Mg-calcite formed in the diamond stability field. Indeed, the postulated prograde subduction trajectory crosses the Dol + Ara = Mg-Cc at pressures close to the graphite–diamond transition (Fig. 9b). One significant problem with using carbonates to deduce metamorphic conditions is that they are often affected by retrograde equilibration. For example, inclusions such as shown in Fig. 9 document a retrograde re-equilibration at temperature of ~700 °C, based on the measured Mg-calcite with $X(\mathrm{Ca}) = 0.88$ coexistent with dolomite.

Finally, our experimental results have some first-order implications to understand CO_2 recycling in subducted crust. For example, Kerrick and Connolly (2001) modeled CO_2 liberation in deeply subducted sediments using phase diagram calculations in the pressure–temperature range up to 6 GPa, 1000 °C without taking the reaction

of Ara + Dol = Mg-Calcite into consideration. Our study shows that Mg-Cc is a relevant phase for hot subduction geotherms (Syracuse et al. 2010) where it would occur at subarc pressures. Mg-Cc has a much larger compositional variability than dolomite or aragonite. Consequently, many de-carbonation reactions in subducted sediments, impure marbles, or altered oceanic crust will be continuous leading to CO_2 release over extended *P–T* sections during subduction metamorphism. In the simple system experiments, Fe has not been considered, but our preliminary experiments show that Fe expands the stability field of Mg-Cc down temperature for at least 50 °C. Thus, for CO_2 liberation in subducted sediments and altered oceanic crust, phase and melting relations have to take Fe–Mg-calcite into consideration (Franzolin et al. 2011; Poli 2015).

Conclusions

A petrogenetic grid for marbles has been determined based on piston cylinder experiments in the system $CaCO_3$–$CaMg(CO_3)_2$. The dissociation of dolomite to aragonite + magnesite has a pronounced positive slope and ends at an invariant point at ~1000 °C, 7.5 GPa. This marks the maximum pressure for the stability of dolomite. The reaction of dolomite + aragonite to Mg-calcite extends from the invariant point to lower *P–T* conditions and is likely relevant for carbonates in hot subduction zones. The composition of Mg-calcite coexistent with aragonite is a good barometer, and coexistent with dolomite is a good thermometer in UHP rocks. With increasing temperature, the degree of disorder in dolomite increases gradually. A rapid increase to complete disorder is observed when the critical curve marking the closure of the solvus between Mg-calcite and dolomite is passed at 1000–1050 °C. Fully disordered carbonates did not order during the fast quenching of the piston cylinder experiments.

Acknowledgments We would like to thank B. Hibberson for assistance with experiments, A. Pawley and B. Luth for helpful reviews, and H. Keppler for handling of the paper. This work has been financially supported by the Australian Research Council.

References

Antao SM, Mulder WH, Hassan I, Crichton WA, Parise JB (2004) Cation disorder in dolomite, $CaMg(CO_3)_2$, and its influence on the aragonite plus magnesite < - > dolomite reaction boundary. Am Mineral 89:1142–1147

Becker H, Altherr R (1992) Evidence from ultra-high-pressure marbles for recycling of sediments into the mantle. Nature 358:745–748

Bischoff WD, Bishop FC, Mackenzie FT (1983) Biogenically produced magnesian calcite inhomogeneities in chemical and physical-properties comparison with synthetic phases. Am Mineral 68:1183–1188

Bundy FP, Strong HM, Bovenkerk HP, Wentorf RH (1961) Diamond-graphite equilibrium line from growth and graphitization of diamond. J Chem Phys 35:383–391

Buob A, Luth RW, Schmidt MW, Ulmer P (2006) Experiments on $CaCO_3$–$MgCO_3$ solid solutions at high pressure and temperature. Am Mineral 91:435–440. doi:10.2138/am.2006.1910

Byrnes AP, Wyllie PJ (1981) Subsolidus and melting relations for the join $CaCO_3$–$MgCO_3$ at 10 kbar. Geochim Cosmochim Acta 45:321–328. doi:10.1016/0016-7037(81)90242-8

Caldeira K (1991) Continental-pelagic carbonate partitioning and the global carbonate-silicate cycle. Geology 19:204–206

Castelli D, Rolfo F, Groppo C, Compagnoni R (2007) Impure marbles from the UHP Brossasco-Isasca unit (Dora-Maira Massif, western Alps): evidence for Alpine equilibration in the diamond stability field and evaluation of the $X(CO_2)$ fluid evolution. J Metamorph Geol 25:587–603

Dobrzhinetskaya LF, Liu ZX, Cartigny P, Zhang JF, Tchkhetia D, Hemley RJ, Green HW (2006) Synchrotron infrared and Raman spectroscopy of microdiamonds from Erzgebirge, Germany. Earth Planet Sci Lett 248:340–349

Franzolin E, Schmidt MW, Poli S (2011) Ternary Ca–Fe–Mg carbonates: subsolidus phase relations at 3.5 GPa and a thermodynamic solid solution model including order/disorder. Contrib Mineral Petrol 161:213–227. doi:10.1007/s00410-010-0527-x

Goldsmith JR, Newton RC (1969) *P–T–X* relations in the system CaCO3–MgCO3 at high temperatures and prssures. Am J Sci 267:160–190

Goldsmith JR, Graf DL, Heard HC (1961) Lattice constants of the Calcium–Magnesium carbonates. Am Mineral 46:453–457

Hammouda T, Andrault D, Koga K, Katsura T, Martin AM (2011) Ordering in double carbonates and implications for processes at subduction zones. Contrib Mineral Petrol 161:439–450. doi:10.1007/s00410-010-0541-z

Hermann J, Rubatto D, Korsakov A, Shatsky VS (2001) Multiple zircon growth during fast exhumation of diamondiferous, deeply subducted continental crust (Kokchetav massif, Kazakhstan). Contrib Mineral Petrol 141:66–82

Hunter BA (1998) Rietica—a visual rietveld program. Comm Powder Diffr Newslett 20:21

Irving AJ, Wyllie PJ (1975) Subsolidus and melting relationships for calcite, magnesite and join $CaCO_3$–$MgCO_3$ to 36 Kb. Geochim Cosmochim Acta 39:35–53. doi:10.1016/0016-7037(75)90183-0

Kelemen PB, Manning CE (2015) Reevaluating carbon fluxes in subduction zones, what goes down, mostly comes up. Proc Natl Acad Sci USA 112:E3997–E4006. doi:10.1073/pnas.1507889112

Kerrick DM, Connolly JAD (2001) Metamorphic devolatilization of subducted marine sediments and the transport of volatiles into the Earth's mantle. Nature 411:293–296

Korsakov AV, Hermann J (2006) Silicate and carbonate melt inclusions associated with diamonds in deeply subducted carbonate rocks. Earth Planet Sci Lett 241:104–118

Luth RW (2001) Experimental determination of the reaction aragonite plus magnesite = dolomite at 5 to 9 GPa. Contrib Mineral Petrol 141:222–232

Martinez I, Zhang JZ, Reeder RJ (1996) In situ X-ray diffraction of aragonite and dolomite at high pressure and high temperature: evidence for dolomite breakdown to aragonite and magnesite. Am Mineral 81:611–624

Morlidge M, Pawley A, Droop G (2006) Double carbonate breakdown reactions at high pressures: an experimental study in the system CaO–MgO–FeO–MnO–CO_2. Contrib Mineral Petrol 152:365–373. doi:10.1007/s00410-006-0112-5

Ogasawara Y, Zhang RY, Liou JG (1998) Petrogenesis of dolomitic marbles from Rongcheng in the Su-Lu ultrahigh-pressure

metamorphic terrane, eastern China. Isl Arc 7:82–97. doi:10.1046/J.1440-1738.1998.00177.X

Ogasawara Y, Ohta M, Fukasawa K, Katayama I, Maruyama S (2000) Diamond-bearing and diamond-free metacarbonate rocks from Kumdy-Kol in the Kokchetav Massif, northern Kazakhstan. Isl Arc 9:400–416

Poli S (2015) Carbon mobilized at shallow depths in subduction zones by carbonatitic liquids. Nat Geosci 8:633–636. doi:10.1038/NGEO2464

Proyer A, Rolfo F, Zhu YF, Castelli D, Compagnoni R (2013) Ultrahigh-pressure metamorphism in the magnesite plus aragonite stability field: evidence from two impure marbles from the Dabie-Sulu UHPM belt. J Metamorph Geol 31:35–48. doi:10.1111/jmg.12005

Reeder RJ (1983) Crystal chemistry of the rhombohedral carbonates. In: Reeder RJ (ed) Carbonates: mineralogy and chemistry, vol 11. Mineralogical Society of America, Washington, DC, pp 1–47

Reeder RJ, Wenk HR (1983) Structure refinements of some thermally disordered dolomites. Am Mineral 68:769–776

Sato K, Katsura T (2001) Experimental investigation on dolomite dissociation into aragonite plus magnesite up to 8.5 GPa. Earth Planet Sci Lett 184:529–534. doi:10.1016/S0012-821x(00)00346-0

Schultz-Güttler R (1986) The influence of disordered, non-equilibrium dolomites on the Mg-solubility in calcite in the system $CaCO_3$–$MgCO_3$. Contrib Mineral Petrol 93:395–398. doi:10.1007/BF00389397

Shatsky VS, Sobolev NV, Vavilov MA (1995) Diamond-bearing metamorphic rocks of the Kokchetav Massif (Northern Kazakhstan). In: Wang X, Coleman RG (eds) Ultrahigh pressure metamorphism. Cambridge University Press, Cambridge, pp 427–455

Shirasaka M, Takahashi E, Nishihara Y, Matsukage K, Kikegawa T (2002) In situ X-ray observation of the reaction dolomite = aragonite plus magnesite at 900–1300 K. Am Mineral 87:922–930

Sobolev NV, Shatsky VS (1990) Diamond inclusions in garnets from metamorphic rocks: a new environment for diamond formation. Nature 343:742–746

Stepanov AS, Rubatto D, Hermann J, Korsakov AV (2016) Contrasting *P–T* paths within the Barchi-Kol UHP terrain (Kokchetav Complex): implications for subduction and exhumation of continental crust. Am Mineral 101:788–807. doi:10.2138/am-2016-5454

Syracuse EM, van Keken PE, Abers GA (2010) The global range of subduction zone thermal models. Phys Earth Planet In 183:73–90. doi:10.1016/j.pepi.2010.02.004

Zhang L, Ellis DJ, Arculus RJ, Jiang W, Wei C (2003) Forbidden zone subduction of sediments to 150 km depth—the reaction of dolomite to magnesite plus aragonite in the UHPM metapelites from western Tianshan, China. J Metamorph Geol 21:523–529. doi:10.1046/J.1525-1314.2003.00460.X